

Electron Thermal Transport Barrier and Density Fluctuation Reduction in a Toroidal Helical Plasma

A. Fujisawa,¹ H. Iguchi,¹ T. Minami,¹ Y. Yoshimura,¹ H. Sanuki,¹ K. Itoh,¹ S. Lee,¹ K. Tanaka,¹ M. Yokoyama,¹
M. Kojima,¹ S.-I. Itoh,² S. Okamura,¹ R. Akiyama,¹ K. Ida,¹ M. Isobe,¹ S. Morita,¹ S. Nishimura,¹ M. Osakabe,¹
A. Shimizu,¹ C. Takahashi,¹ K. Toi,¹ Y. Hamada,¹ K. Matsuoka,¹ and M. Fujiwara¹

¹National Institute for Fusion Science, Oroshi-cho, Toki-shi, 509-52 Japan

²RIAM, Kyushu University, Kasuga, 816 Japan

(Received 16 October 1998)

A thermal transport barrier resulting in a high central electron temperature of ~ 2 keV is established in the core of electron-cyclotron-resonance heated plasmas of the Compact Helical System Heliotron/Torsatron. The formation of the barrier is correlated with the reduction in the density fluctuations and with a structural change of the radial electric field profile at the barrier location. The results suggest that the decrease in fluctuation should contribute to a reduction of anomalous transport and a drastic increase in electron temperature at the barrier. [S0031-9007(99)08825-0]

PACS numbers: 52.25.Fi, 52.35.Nx, 52.55.Hc, 52.70.-m

The formation mechanism of transport barriers in the plasma periphery and the interior [1–6] that is associated with the transition to improved confinement modes is an important issue to be addressed. The impacts of the derivative of a radial electric field (E_r shear) have been theoretically suggested as a cause of the fluctuation suppression leading to the reduction of a fluctuation-driven transport at the barrier location [7–12]. A good correlation between the low fluctuation level and the excellent transport property has been experimentally shown in negative magnetic shear modes of several tokamaks [13,14]. The effects of E_r shear, as well as a favorable change of the magnetic field structure, on the formation of internal transport barriers have also been reported in improved confinement modes [15–19].

In toroidal helical plasmas that are nearly a current-free configuration, strong E_r shear can be caused by its own bifurcation nature. Neoclassical theory for toroidal helical plasmas predicts two solutions with different electric fields due to helical ripple losses [20,21]. In the Compact Helical System (CHS) Heliotron/Torsatron [22], a strong E_r shear is produced by using electron-cyclotron-resonance (ECR) heating [23,24]. There an internal transport barrier for an electron has been recently observed. Both density fluctuation spectrum and the fine structure of E_r , using the Heavy Ion Beam Probe (HIBP), have been directly measured around the barrier location, with sufficient temporal and spatial resolution. This paper presents the first observation of an internal transport barrier for electrons in a toroidal helical plasma, together with the density fluctuation reduction, particularly of low frequency waves of < 50 kHz, exactly at the barrier point that has the maximum E_r shear.

The CHS is a medium size device whose major and averaged minor radii are 1.0 and 0.2 m, respectively. The presented experiments are performed at the axis magnetic field strength of 0.88 T, where the gyrotron

frequency of 53.2 GHz has a resonance exactly on the axis. The line-averaged density is rather low about $\bar{n}_e \approx (3-4) \times 10^{12} \text{ cm}^{-3}$. The cesium beam energy is 72 keV for the HIBP measurements under this operational condition. The radial length of the sample volume is a few cm according to a trajectory calculation. The detected beam current is ~ 100 nA at maximum, while the amplifier noise level is approximately ± 0.2 nA. The time resolution is up to 250 kHz.

Density fluctuation can be known from the detected beam intensity I_D of the HIBP that is expressed as $I_D(r) \propto Q_{12}(r) \exp[-\alpha_1(r) - \alpha_2(r)] \Delta V$. Here, $Q_{12}(r) (\equiv n_e \langle \sigma v \rangle_{12} v_B^{-1})$ is the local rate of beam ionization from singly to doubly charged states, $\langle \sigma v \rangle_{12} v_B^{-1}$, v_B , and ΔV are the effective cross section, the beam velocity, and the sample volume, respectively. The beam attenuation factor α is defined as $\alpha_i(r) \equiv \int_r Q_i dl_i$, where $Q_i (i = 1, 2)$ is the total ionization rate from the i th charged states to a more highly charged state. The ionization rate is proportional to the electron density [e.g., $Q_{12}(r) \propto n_e(r)$] provided that the electron temperature is sufficiently high (~ 100 eV).

Then the intensity fluctuation is expressed by $\delta I_D(r)/I_D(r) = \delta n_e(r)/n_e(r) - \delta \alpha_1(r) - \delta \alpha_2(r)$. If the second and third terms on the right-hand side are negligible compared to the first term, the intensity fluctuation mainly reflects the local density fluctuation. The condition is reduced into $\bar{n}_e \ll (\sum \langle \sigma v \rangle_i v_B^{-1} L_i)^{-1}$, where L_i and \bar{n}_e represent the path lengths of primary ($i = 1$), or secondary ($i = 2$) beams, and the line-averaged density, respectively. According to the ionization rate based on Lotz's empirical formula [25], the local density fluctuation can be measured when the density is lower than $\bar{n}_e \sim 5 \times 10^{12} \text{ cm}^{-3}$.

Potential profiles are obtained using the HIBP for ECR heated plasmas with a different power of $P_{ECH} = 150$ kW and 200 kW, as is shown in Fig. 1a. For

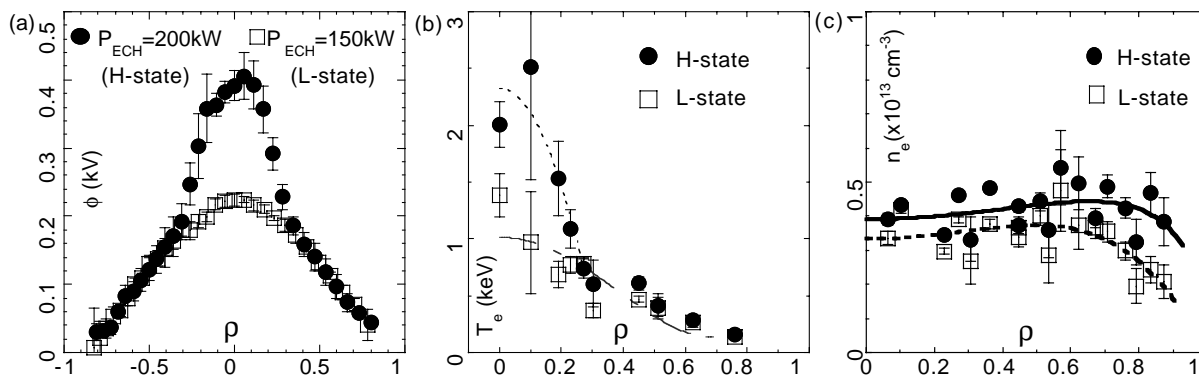


FIG. 1. (a) Potential profiles with different ECH powers. The circles and squares show the potential profiles with the power of 200 kW (*H* state) and 150 kW (*L* state), respectively. (b) Electron temperature profiles for *H* and *L* states. (c) Density profiles for the *H* and *L* states. The line-averaged densities are $n_e = 4 \times 10^{12} \text{ cm}^{-3}$ and $n_e = 3 \times 10^{12} \text{ cm}^{-3}$ for the *H* and *L* states, respectively.

convenience, the states of $P_{\text{ECH}} = 150 \text{ kW}$ and $P_{\text{ECH}} = 200 \text{ kW}$ are termed “*L*” states and “*H*” states, respectively. The potential profile of the *H* state exhibits a prominent peak (or a dome) around the core that is not seen in the *L* state. The power threshold for the transition was found to be in the range of approximately $\sim 150\text{--}170 \text{ kW}$ in the density regime of $\bar{n}_e \approx (3\text{--}4) \times 10^{12} \text{ cm}^{-3}$. The gradient of the potential (or E_r) inside of $\rho \approx 0.25$ is considered to bifurcate into a branch of higher value. The plasma rotation due to $\mathbf{E} \times \mathbf{B}$ velocity is clearly different inside and outside this point; $v_{\mathbf{E} \times \mathbf{B}}^{\text{out}} \sim 9 \text{ km/s}$, and $v_{\mathbf{E} \times \mathbf{B}}^{\text{in}} \sim 2 \text{ km/s}$.

Thomson scattering measurements reveal a clear difference of electron temperature profiles in these two states. Figure 1b presents electron temperature T_e profiles. The circles and squares show the T_e profiles with the *H* and *L* states, respectively. The electron temperatures are obtained by a statistical average in a few dozen shots with an identical operational condition since the scattering light is not so sufficient in this low density regime. The central temperature of the *H* state is $2.0 \pm 0.2 \text{ keV}$, while that of the *L* state is $1.4 \pm 0.1 \text{ keV}$. The T_e profiles outside of the normalized radius of $\rho = 0.27$ are almost the same for both states. The drastic change of the temperature gradient occurs at $\rho = 0.25$, and there the T_e gradients are estimated as $dT_e/dr = -0.57 \text{ keV/cm}$ and $dT_e/dr = -0.12 \text{ keV/cm}$ for the *H* and *L* states, respectively.

Figure 1c shows the n_e profiles measured with the Thomson scattering system. The n_e profiles have a flat or slightly hollow shape for both cases. The line-averaged densities in the *H* and *L* states are $\bar{n}_e = 4 \times 10^{12} \text{ cm}^{-3}$ and $\bar{n}_e = 3 \times 10^{12} \text{ cm}^{-3}$, respectively. Around $\rho \approx 0.25$, where the steep T_e gradient exists, no significant change can be seen in the density. The drastic change in pressure gradient, consequently, exists at $\rho = 0.25$ for the *H* state. Therefore, an energy transport barrier for electrons is formed at the normalized radius of $\rho \approx 0.25$.

A fine structure of potential has been investigated around this barrier point. Figure 2 shows a

typical example of the measurements with a spatial resolution of 2 mm. The electric field can be expressed by a form of $\tanh[(\rho - \rho_0)/\alpha]$. Then the potential profile takes the following function form: $\phi(\rho) = A \ln[\cosh[(\rho - \rho_0)/\alpha] + B\rho + C]$, where A , B , C , ρ_0 , and α are the fitting parameters. By fitting this function to the data in Fig. 2a, we have obtained the following results: $A = 0.028$, $\alpha = 0.047$, $\rho_0 = 0.259$, and $B = -0.891$. Figure 2b shows the obtained E_r and its shear as a function of a normalized minor radius. The E_r values inside and outside of the barrier are $7.8 \pm 0.7 \text{ kV/m}$ and $1.7 \pm 0.3 \text{ kV/m}$, respectively. In a real dimension, the full width at half maximum and the

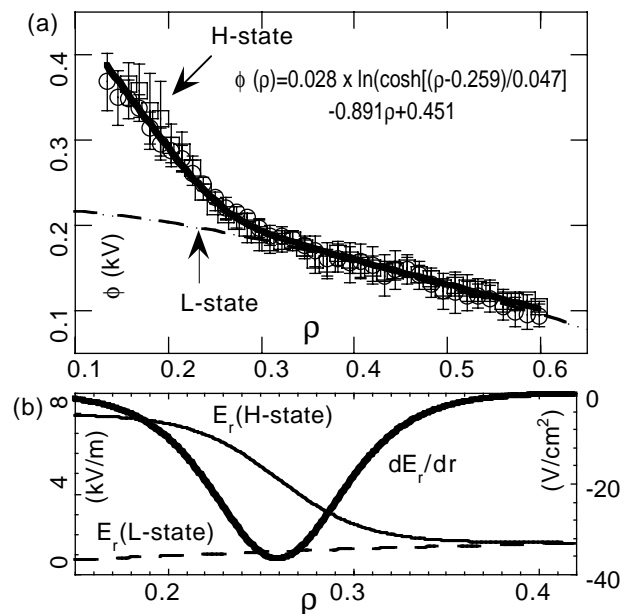


FIG. 2. Precise measurements around the barrier location using an HIBP. (a) Fine structure of potential around the barrier point. Here two data sets from sequential shots are plotted and used for the fitting process. (b) Deduced E_r structure and its shear. Profiles of the potential and E_r of the *L* state are shown as a reference.

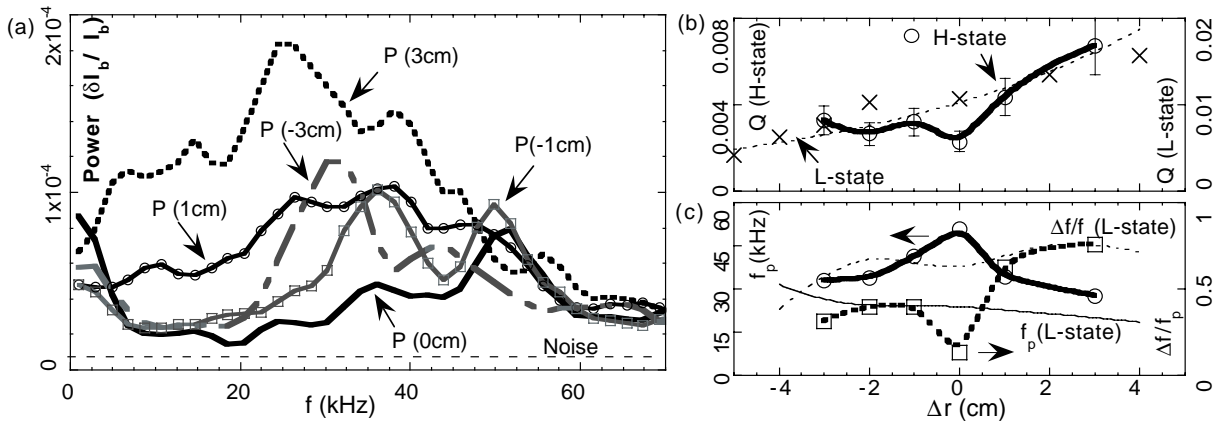


FIG. 3. (a) Power spectra of density fluctuation at several points around the shear-maximum point in the H state. (b) Integrated fluctuation powers. The circles and \times marks represent those of the H and L states, respectively. (c) Peak f_p and width Δf of frequency spectrum. The circles (thin line) and squares (thin dashed line) show the peak and normalized bandwidth in the H state (L state), respectively. Δr represents the distance from the shear-maximum point.

barrier position from the plasma center are 1.3 ± 0.5 cm and 4.7 ± 0.4 cm, respectively. The resulting E_r shear is $\sim 39.7 \pm 17.4$ V/cm².

Density fluctuation around the shear-maximum point is measured shot by shot in the sequential discharges under the identical operation condition with the cases of Fig. 2. The fluctuation spectra of the detected beam current from several spatial points for the H state are illustrated in Fig. 3a: $\Delta r = -3, -1, 0, 1,$ and 3 cm, where Δr represents the distance from the shear-maximum point, and $\Delta r = 0$ corresponds to $r_0 = 4.3 \pm 0.9$ cm ($\rho_0 = 0.23 \pm 0.05$) here. The spectrum at $\Delta r = 0$ cm shows a reduction in power whose frequency ranges from 5 to 70 kHz, while the other spectra have a larger power.

Figure 3b shows the integral of power spectrum from 5 to 70 kHz as a function of the observed position: $Q(\Delta r) = \int P df$. The figure clearly demonstrates power reduction at the shear-maximum point by 39%, which is estimated from $[Q(1 \text{ cm}) - Q(0)]/Q(1 \text{ cm})$ with $Q(1 \text{ cm}) = 0.5[Q(1 \text{ cm}) + Q(-1 \text{ cm})]$. Figure 3c shows a peak frequency and width of spectrum normalized by the peak frequency. Those values are obtained by fitting the function of $P(f) = P_0 \exp[-(f - f_p)^2/\Delta f^2] + P_{\text{base}}$, to the spectrum around the peak, where P_{base} , P_0 , f_p , and Δf are the fitting parameters. Figure 3c shows that the peak frequency has a maximum and the normalized width becomes narrower at the shear-maximum point. Figure 3c indicates that the waves with lower frequency suffer a more effective reduction.

The integral is performed from 5 to 70 kHz. This is because the low frequency should contain other effects such as plasma movements, and the power spectrum above 70 kHz just shows a nature of *white noise* that corresponds to the parameter $P_{\text{base}} \sim 1 \times 10^{-5}$. This fluctuation level could be mainly ascribed to the path integral effects [26,27]. The fluctuations independent along the beam orbit contribute to the base level of the

fluctuation in the beam intensity. The noise level of an integral fluctuation can be assumed to be $Q_{\text{noise}} \approx 70 \times 10^{-5}$. Then the reduction of fluctuation power at the shear-maximum point is 48%, if the integral fluctuation level subtracted by the noise is used for the estimation.

The integral of power spectrum is also shown in Fig. 3b for the L state. In this state, the fluctuation increases monotonically toward the plasma edge. The power level is approximately twice as large as the H state; thus, the absolute value of fluctuation is $\sim \sqrt{2}$ times larger. The difference in the fluctuation level should be ascribed to the lower density in the L state. Figure 3c also plots the peak frequency of the L state, which is obtained in the same manner. The frequency (~ 20 kHz) does not show any significant change, being different from the H state.

In another set of discharges with $\bar{n}_e = 3.5 \times 10^{12}$ cm⁻³, E_r shear of 34 ± 10 V/cm² is obtained in a potential profile with a dome (H state) when $P_{\text{ECH}} = 170$ kW is applied. In this case, the fluctuation spectra around the shear maximum show a peak about ~ 15 kHz with the bandwidth of 20 kHz. The observed fluctuation reduction is by 26% and 28% according to the definition without and with consideration of the noise level; $Q(1) = 9.2 \times 10^{-3}$ and $Q(0) = 6.8 \times 10^{-3}$. This reduction is mainly caused by a decrease in the fluctuation power around the peak frequency. The background fluctuation level of $Q(1 \text{ cm})$ is almost the same as that of the L state. Therefore, the fluctuation reduction is correlated with the existence of the E_r shear.

According to a neoclassical theory [21], the electron heat flux at the shear-maximum point ($\rho \sim 0.25$) is estimated as $q^{\text{neo}} \sim (1-2) \times 10^4$ W/m² in the L state, when the available parameters of T_e , n_e , and E_r are taken into account. The experimental electron heat flux in this case is, however, roughly estimated as $q^{\text{exp}} \sim 1 \times 10^5$ W/m². On the other hand, the neoclassical electron heat flux can become closer to the level of the experimental value in the H state due to the higher

temperature gradient. The estimation implies that the anomalous transport is reduced at the shear-maximum point. The location of the steep dT_e/dr is in good agreement with the E_r -shear-maximum position within the present error bar. It is suggested that the E_r -shear reduction of fluctuation should, therefore, lessen the anomalous heat transport and form the transport barrier, similar to discussions in the barrier formation of the tokamaks.

However, the polarity of E_r at the CHS transport barrier is opposite of the negative field usually observed in the transport barrier of tokamaks [7]. An exception is the forced H mode using a biasing electrode in the TEXTOR tokamak [28], where density fluctuation reduction is confirmed when the E_r shear is above a critical value ($\sim 60\text{--}70$ V/cm²). The other point is that a structural change of magnetic field, or a negative magnetic shear formation, is an essential factor to establish the internal transport barrier in tokamaks. No significant change of magnetic structure, however, is expected in the CHS case since the induced toroidal current is totally less than 0.5 kA.

Another peculiarity of the CHS transport barrier is that the density profile indicates no gradient change at the barrier location. This is related to the importance of off-diagonal terms for the neoclassical particle flux in the toroidal helical plasma [20,21,29]. The neoclassical calculation gives the particle fluxes of $\Gamma^{\text{neo}} \sim 0.2 \times 10^{20} \text{ m}^{-2} \text{ s}^{-1}$ and $\Gamma^{\text{neo}} \sim 1.5 \times 10^{20} \text{ m}^{-2} \text{ s}^{-1}$ at the barrier location for the L and the H state, respectively. In the H state, a decrease in the fluctuation-driven particle flux could compensate the neoclassical part enhanced by the T_e gradient.

It should also be notified here that in toroidal helical plasmas the absolute value of E_r as well as the E_r shear is important for transports, particularly in collisionless regime. The strongly positive E_r should have better neoclassical transport property than the slightly positive E_r [20,21,29]. Hence, the transition of E_r to the strongly positive branch may potentially contribute to the formation of the internal transport barrier in toroidal helical plasmas.

In the Wendelstein VII-AS, a H -state-like characteristic has been observed in the temperature profile of ECR heated plasmas. The ECH plasma also exhibits the bifurcation nature in electron cyclotron emission (ECE) from the plasma core [29]. The ECE signal reflecting the central electron temperature shows a pulsation, similar to the potential behavior in the CHS plasma [30], to be interpreted as creation and annihilation of the internal transport barrier. Thus, the bifurcation characteristics in electron temperature (or potential) may be common with various toroidal helical plasmas.

In conclusion, we have described several observations associated with the formation of an internal thermal transport barrier for an electron in ECR heated plasmas of the CHS. The present observations show a correlation between the transport barrier formation, fluctuation reduction, and structural change of E_r at the barrier location.

-
- [1] F. Wagner *et al.*, Phys. Rev. Lett. **49**, 1408 (1982).
 - [2] S.-I. Itoh and K. Itoh, Phys. Rev. Lett. **60**, 2276 (1988).
 - [3] K. C. Shaing and E. Crume, Jr., Phys. Rev. Lett. **63**, 2369 (1989).
 - [4] F. M. Levinton *et al.*, Phys. Rev. Lett. **75**, 4417 (1995).
 - [5] E. J. Strait *et al.*, Phys. Rev. Lett. **75**, 4421 (1995).
 - [6] G. M. Stabler *et al.*, Phys. Plasmas **1**, 909 (1994).
 - [7] For a review, see K. Itoh and S.-I. Itoh, Plasma Phys. Controlled Fusion **38**, 1 (1996).
 - [8] S.-I. Itoh and K. Itoh, J. Phys. Soc. Jpn. **59**, 3815 (1990).
 - [9] K. C. Shaing *et al.*, in *Proceedings of the 12th International Conference on Plasma Physics and Controlled Nuclear Fusion Research, Nice, France, 1988* (International Atomic Energy Agency, Vienna, 1989), Vol. 2, p. 13.
 - [10] F. L. Hinton, Phys. Fluids B **3**, 696 (1991).
 - [11] H. Biglari, P. H. Diamond, and P. W. Terry, Phys. Fluids B **2**, 1 (1990).
 - [12] K. Itoh, S.-I. Itoh, A. Fukuyama, H. Sanuki, and M. Yagi, Plasma Phys. Controlled Fusion **36**, 123 (1994).
 - [13] E. Mazzucato *et al.*, Phys. Rev. Lett. **77**, 3145 (1996).
 - [14] E. A. Lazarus *et al.*, Phys. Rev. Lett. **77**, 2714 (1996).
 - [15] R. E. Bell *et al.*, Phys. Rev. Lett. **81**, 1429 (1998).
 - [16] F. M. Levinton *et al.*, Phys. Rev. Lett. **80**, 4887 (1998).
 - [17] A. Fukuyama *et al.*, Plasma Phys. Controlled Fusion **36**, 1385 (1994).
 - [18] K. C. Shaing *et al.*, Phys. Rev. Lett. **80**, 5353 (1998).
 - [19] P. H. Diamond *et al.*, Phys. Rev. Lett. **78**, 1472 (1997).
 - [20] D. E. Hastings, W. A. Houlberg, and K. C. Shaing, Nucl. Fusion **25**, 445 (1985).
 - [21] L. M. Kovrizhnykh, Nucl. Fusion **24**, 435 (1984).
 - [22] K. Matsuoka *et al.*, in *Proceedings of the 12th International Conference on Plasma Physics and Controlled Nuclear Fusion Research, Nice, France, 1988* (Ref. [9]), Vol. 2, p. 411.
 - [23] A. Fujisawa *et al.*, Phys. Rev. Lett. **79**, 1054 (1997).
 - [24] Theoretical prediction of internal transport barrier is discussed in K. Itoh *et al.*, J. Plasma Fusion Res. Suppl. **74**, 282 (1998).
 - [25] W. Lotz, Astrophys. J. Suppl. Ser. **14**, 207 (1967).
 - [26] J. W. Heard *et al.*, Rev. Sci. Instrum. **64**, 1001 (1993).
 - [27] A. Fujisawa *et al.*, Rev. Sci. Instrum. **68**, 3393 (1997).
 - [28] R. R. Weynants, S. Jachmich, and G. Van Oost, Plasma Phys. Controlled Fusion **40**, 635 (1998).
 - [29] R. Brakel *et al.*, Plasma Phys. Controlled Fusion **39**, B273 (1997).
 - [30] A. Fujisawa *et al.*, Phys. Rev. Lett. **81**, 2256 (1998).